Heliyon 10 (2024) e35018

Contents lists available at ScienceDirect

Heliyon

journal homepage: www.cell.com/heliyon

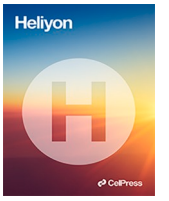

Research article

Fundamental characteristics of ultrasonic green formulations using *Avena sativa* L. extract-mediated gold nanoparticles and electroconductive nanofibers for cardiovascular nursing care

Xinfang Wei [a], Xiaoshan Jiang [b], Hongzan Li [c,*]

[a] *Department of Cardiovascular Medicine CCU, Zhongshan People's Hospital, No. 2 Sunwendong Road, Zhongshan City, Guangdong, 528403, China*
[b] *Department of Geriatrics, Qingdao Chengyang District People's Hospital, No. 600, Changcheng Road, Chengyang District, Qingdao, 266109, Shandong Province, China*
[c] *School of Nursing, Guangdong Medical University, No. 1 Xincheng Road, Songshan Lake Science and Technology Park, Dongguan, Guangdong, 523808, China*

ARTICLE INFO

Keywords:
Cardiovascular nursing care
Gold nanoparticles
Ultrasonic
Avena sativa L.

ABSTRACT

In the pursuit of novel approaches to address chronic heart failure and enhance cardiovascular nursing care, environmentally sustainable nanomaterials have taken center stage. Recent progress in regenerative medicine has opened doors for the use of biocompatible biomaterials that provide mechanical support to damaged heart tissue and facilitate electrical signaling. This study was dedicated to developing advanced electroconductive nanofibers by incorporating eco-friendly *Avena sativa* L. extract-mediated gold nanoparticles (AuNPs) into polyaniline to create an intricate cardiac patch. The AuNPs were synthesized through an environmentally friendly chemical process aided by ultrasonic conditions. Comprehensive physicochemical analyses, such as UV–Vis spectroscopy, SEM, TEM, DPPH assay, and XRD, were carried out to characterize the AuNPs. These AuNPs were then blended with a polycaprolactone/gelatin polymeric solution and electrospun to fabricate cardiac patches, which underwent thorough evaluation using various techniques. The resulting cardiac patch demonstrated excellent hemocompatibility, antioxidant properties, and cytocompatibility, offering a promising therapeutic approach for myocardial infarctions and the advancement of cardiovascular nursing care.

1. Introduction

Cardiovascular diseases (CVDs) are the leading cause of morbidity and mortality in both developed and developing regions. It is estimated that CVDs could lead to 18 million deaths this year, with a potential rise to 23.5 million by 2030, constituting almost 32 % of all worldwide fatalities. Additionally, it is noteworthy that over 80 % of these deaths are linked to acute myocardial infarction (AMI) [1,2]. Atherosclerosis, characterized by the gradual accumulation of fats and fibrous tissue in artery walls, is the primary cause of cardiovascular disease (CVD). This process leads to a compromised immune response and altered cholesterol metabolism, ultimately resulting in the formation of atherosclerotic plaques. The presence of these plaques in the coronary arteries causes narrowing, leading to an imbalance between oxygen demand and supply to the heart muscle. This mismatch results in myocardial ischemia, and if left untreated, can lead to the rupture of these fragile plaques, ultimately resulting in a heart attack. The collective term for this group of

* Corresponding author.
E-mail address: lihongzan123@163.com (H. Li).

https://doi.org/10.1016/j.heliyon.2024.e35018
Received 17 May 2024; Received in revised form 18 July 2024; Accepted 22 July 2024
Available online 25 July 2024

diseases is commonly known as atherosclerotic cardiovascular disease (ASCVD) [3].

The treatment and management of cardiovascular diseases (CVDs) require advanced approaches, involving highly skilled and experienced nurses, specialized facilities, and state-of-the-art medical devices. Cardiac nursing is a focused area within the nursing profession that centers on the comprehensive care and supervision of patients with a variety of cardiovascular conditions. Working under the guidance of cardiologists, cardiac nurses play a pivotal role in the oversight of diverse cardiovascular issues such as unstable angina, cardiomyopathy, coronary artery disease, congestive heart failure, myocardial infarction, and cardiac dysrhythmia. They provide crucial support for patients dealing with these disorders by delivering postoperative care in surgical units, performing stress test evaluations, monitoring cardiac and vascular conditions, and conducting health assessments. Alongside nursing care, the use of advanced treatment options is imperative.

The best method for restoring heart function is through heart transplantation. However, this procedure has faced challenges due to the shortage of organ donors and the potential for post-transplant complications such as infections and malignancies [4,5]. The advent of tissue engineering technology has presented a viable approach for the development of functioning cardiac tissues that have the potential to be transplanted for the treatment of myocardial dysfunction. Several techniques have been explored to create three-dimensional cardiac tissues in vitro. One approach includes developing biomimetic matrix systems for tissue production, using methods like hydrogels, prefabricated matrices, decellularized heart tissues, and cell sheets [6–8]. Various techniques in tissue engineering for the heart, including utilizing 3D hydrogels to craft large-scale cardiac structures, functionalizing cardiac tissues with highly decellularized heart tissue, and creating thicker cardiac patches with multi-layer cell sheets, have displayed promising potential. However, it's crucial to acknowledge that these methods have their limitations. For instance, hydrogel systems may lack sufficient mechanical strength and suturability, while decellularized systems could encounter production challenges and immune responses. Additionally, the process of growing 3D tissues through cardiac cell sheet techniques can be laborious and resource-intensive [9]. Pre-made matrices, like nanofibrous and microporous scaffolds, have become a promising solution for addressing the challenges in cardiac tissue engineering. Lately, there has been increasing enthusiasm for using nanofibrous scaffolds created through electrospinning as a means to engineer functional cardiac tissues [10–12]. This is primarily due to the fact that these scaffolds possess structures that closely resemble the extracellular matrix (ECM) of the native myocardium. Additionally, they exhibit exceptional mechanical properties, allow for convenient adjustment of fiber characteristics, facilitate effective material handling and suturing during implantation, and can be produced on a large scale.

Significantly, progress in developing electrospun scaffolds with intricate structures (such as aligned, spring-like fibers) and diverse compositions (incorporating biomolecules and nanoparticles) has rendered them remarkably versatile for enhancing the organization and functions of cardiac tissues [13–16]. One instance of this is the use of aligned conductive electrospun polyaniline (PANi)/poly (lactic-co-glycolic acid) (PLGA) scaffolds, which have been demonstrated to promote the organization and connectivity of cardiomyocytes in cardiac tissues. Furthermore, these scaffolds have shown the ability to induce synchronized beating of the cardiomyocytes when subjected to electrical stimulation [17]. Electrospun scaffolds have demonstrated significant promise in the field of cardiac tissue engineering, as they possess the ability to facilitate the development of engineered cardiac tissues in vitro. Moreover, these scaffolds offer crucial initial structural and conductive support, thereby enabling the sustained contraction of these tissues following their implantation *in vivo*.

Additionally, it is feasible to enhance the effectiveness of the nanofibrous cardiac patch by integrating AuNPs into/onto the patch. As part of the fabrication process, gold nanowires were integrated into the pore walls of 3D macroporous alginate scaffolds. When cardiomyocytes were cultured within the scaffolds, interactions between the cells and the wires were observed, leading to a significantly improved electrical signal transmission in the engineered tissue. This enhancement was distinguished by increased speed and synchronization, surpassing the performance of tissues grown in unmodified scaffolds [18,19]. In the current assay, we fabricated nanofiborus cardiac patch bearing green synthesized AuNPs to improve efficacy of cardiac nursing care [20,21]. The present study is the first report on the combination of the *Avena sativa* L. Extract-mediated AuNPcs with Polycaprolactone (PCL) nanofibers to fabricate cardiac patch. Previous studies may have evaluated each compound separately, but we combined the green chemistry approach with electrospinning technique to fabricate a sophisticated and innovative treatment strategy.

2. Materials and methods

2.1. Chemical and reagents

Potassium tetrachloroaurate (III), ($KAuCl_4$) and PCL (Mw = 80,000 g mol^{-1}) were obtained from Sigma–Aldrich (St. Louis, U.S.A). The solvents hydrochloric acid (HCl), chloroform, dimethyl sulfoxide (DMSO), and methanol were obtained from Merck (Darmstadt, Germany). DMEM/F-12 cell culture medium, MTT powder, Trypsin- EDTA, Penicillin–Streptomycin (Pen-Strep), anf Fetal Bovine Serum (FBS) were obtained from Gibco (Thermo Fisher Scientific, Dreieich, Germany). All other chemicals were of analytical grade and used without further purification unless otherwise noted.

2.2. Plant extraction

The extraction was conducted according to previous study [22]. Dust, impurities, and contaminants of the plant were removed by a series of washing steps (twice with 0.1 M HCl solution and afterward rinsed three times with deionized (DI) water). Then, about 150 g of the washed plant was added to boiling distilled water and heated for 4 h at 80 °C under rigorous stirrer. Using a Whatman filter paper grade 01 (pore size 25 μm), the obtained extract was filtered and stored a refrigerator at 4 °C for further experimental work.

2.3. Synthesis of AuNPs

The AuNPs were synthesized via a green chemistry synthesis approach [23]. In this concept, the extract is applied as the reducing agent of gold salt and capping agent of the final NPs. The reaction mixture (10 mL of the extract and 90 mL of 0.1 mM $KAuCl_4$) was heated at 90 °C under rigorous for 24 h. Then, the reaction mixture was centrifuged at 4000 rpm and the resulting supernatant (containing the AuNPs) was collected and stored for further analysis and use.

2.4. Characterization of AuNPs

2.4.1. Morphology

The morphology of the synthesized AuNPs was evaluated using scanning electron microscope (SEM) and Transmission Electron Microscopy (TEM) instrument. The sample preparation was conducted by distributing a drop of colloidal AuNPs (20 μL) onto the copper grid, followed by drying at room temperature inside a desiccator.

2.4.2. Hydrodynamic size and zeta potential

Using the dynamic light scattering (DLS) technique, the particle size, size distribution, and the zeta potential of AuNPs were evaluated. The experiments were conducted on one mL of a diluted samples.

2.4.3. Crystallinity

The crystallinity of the AuNPs was evaluated using a Bruker D2 PHASER instrument, running at 30 kV voltage and 10 mA current, utilizing Cu-Kα radiation (1.5418 Å) at 40 kV acceleration voltages. The experiment was conducted on vacuum dried sample of AuNPs colloidal solution.

2.4.4. Optical property

The UV–Visible Spectrophotometer (UV-2450, Shimadzu, Japan) was employed to quantify the absorption band of Surface Plasmon Resonance (SPR) in green synthesized AuNPs. The measurements were carried out in the wavelength range of 400–600 nm.

2.5. Fabrication of the nanofibrous cardiac patch

The nanofibrous cardiac patch was fabricated using the electrospinning method. At first, the polymeric solution containing AuNPs was prepared. In this research, a solution with a PCL concentration of 10 % w/v was formulated by dissolving 500 mg of PCL powder in 500 mL of a mixture of chloroform and methanol (3:1 v/v). The solution was then stirred for 24 h (h) at room temperature, following procedures outlined in previous studies [24,25]. Following this, a solution containing 5.0 % (w/v) of AuNPs was added to the mixture and stirred for an additional 24 h before initiating the electrospinning process. The electrospinning process of the polymer solution was carried out using a specially designed setup consisting of a KD Scientific Flow Rate apparatus and an ES 50P-10W Gamma High Voltage system. The electrospinning parameters were pre-optimized and included a flow rate of 0.8 mL/h, a voltage of 18 kV, a tip-to-collector distance of 10 cm, and a needle size of 20 G (0.91 mm).

2.6. Characterization of the nanofibrous cardiac patch

2.6.1. Morphology observation

The morphology of the nanofibrous cardiac patch was visualized using SEM imaging technique. To prepare the sample, a short segment of a patch was mounted on a brass stub with double adhesive tape and sputter-coated with gold in a vacuum using a Sputter Coater (Leica EM SCD005 in Wetzlar, Germany). The specimens were then observed at the accelerating voltage of 20 kV. The nanofiber diameters were measured randomly using ImageJ Software (Version 1.52a by NIH in Bethesda, MD, USA).

2.6.2. Wettability assessment

The wettability of the nanofibers was evaluated by measuring the water contact angle using the drop method, where deionized water was placed on the surfaces of the nanofibers. The experimental procedure involved doing the measurements three times and calculating the mean value of the contact angle.

2.6.3. Porosity measurement

The liquid displacement method is a technique used in scientific experiments to determine the volume of an object by measuring the volume of liquid it displaces. In this experimental procedure, scaffolds of known weight were immersed in a liquid medium that exhibited no dissolution or swelling effects on the nanofibers. Ethanol, being a nonpolar solvent, exhibits minimal interaction with polymeric fibers, hence facilitating its penetration into the mat and complete occupation of all sample pores. Consequently, it enables the determination of the total volume of pores. The mass of the nanofiber mats was quantified before to and subsequent to their immersion in ethanol. The calculation of porosity was performed utilizing the subsequent equation.

$$P\,(\%) = \frac{(ma - mp)/pa}{(ma - mp)/Pa + mp/Pp} \times 100$$

In the given context, the variables “ma,” “mp,” "ρa," and "ρp" represent the mass of saturated material, the mass of dried material, the density of the liquid (specifically ethanol), and the density of the polymer, respectively.

2.6.4. Water absorption measurement

The evaluation of cardiac patches often involves the assessment of the swelling ratio, a significant criterion. Typically, the gravimetric method is employed to conduct this testing. In this study, the nanofiber membranes were sectioned into dimensions of 3 × 3 cm and afterward submerged in phosphate-buffered saline (PBS) with a pH of 7.4 and maintained at a temperature of 37 ± 1 °C. At regular intervals, the membranes were extracted and placed onto a filter paper in order to eliminate any moisture that had stuck to their surfaces prior to being weighed. The findings were presented in the form of timeline charts, indicating the swelling ratio (SR%) values. The measurements were conducted in triplicate.

2.7. Biological evaluations

2.7.1. Antioxidant assays

The antioxidant potential of the synthesized AuNPs was evaluated using their radical scavenging activity against DPPH, H_2O_2, and ONOO. According to the previous studies [26], different concentration of AuNPs (2, 4, 6, 8, 12, 24, and 40 μg/mL) were incubated with the DPPH (2.7 mL of 2.5 mM) at 37 °C for 20 min and the absorbance of the solution was read at 517 nm. According to the previous studies [27], different concentration of AuNPs (2, 4, 6, 8, 12, 24, and 40 μg/mL) were incubated with hydrogen per oxide (0.6 mL, 50 mM) at 37 °C for 10 min and the absorbance of the solution was read at 230 nm.

2.7.2. Release profile

The investigation focused on studying the release patterns of AuNPs from nanofibers in phosphate-buffered saline (PBS) solution with a pH of 7.4. The cardiac patch incubated in 50 mL PBS at a temperature of 37 °C. Samples of 2 mL were extracted from the release medium at various time intervals until the release process reached completion. Following this, an equivalent amount of fresh PBS was introduced as a replacement. The samples underwent centrifugation at 10,000 revolutions per minute for 10 min at room temperature. Following this, the liquid portion above the sediment, referred to as the supernatant, was meticulously transferred to a cuvette. The supernatant was then analyzed using a UV/vis spectrophotometer.

2.7.3. Hemocompatibility assay

A total of 2 mL of freshly anticoagulated blood collected from human volunteers was mixed with 2.5 mL of normal saline solution. For the test samples, a volume of 0.2 mL of diluted blood was employed. The mixture was maintained at a temperature of 37 °C for 60 min, followed by centrifugation at 1500 rpm for 5 min. The liquid component of the sample was transferred to a 96-well plate, and light absorption readings were taken at a wavelength of 545 nm using a BioTek Synergy 2 Multi-Mode Microplate Reader. The average of three measurements was calculated. Positive controls were prepared by diluting 0.2 mL of blood in 10 mL of deionized water, while negative controls were prepared by diluting 0.2 mL of blood in 10 mL of normal saline. The extent of hemolysis was determined using a specific equation.

2.7.4. Cytocompatibility assay

The viability of the cells under incubation with the patches was evaluated using the MTT assay. The patches were sterilized by immersing them in a 70 % (v/v) ethanol solution for 30 min at room temperature. They were then exposed to ultraviolet light for an additional 30 min. Cell viability on the scaffolds was evaluated using the MTT assay. The experiment involved 6 samples per group to ensure technical replication. Cells were seeded onto the scaffolds at a density of 8×10^3 cells per sample. At 48 h after incubation, the cell culture medium was replaced with 100 μL of MTT solution (0.5 mg/mL in PBS), followed by incubation at 37 °C for 4 h. Afterward, the MTT solution was carefully replaced with 100 μL of DMSO. The plates were gently agitated until the dark blue formazan crystals dissolved completely. The absorbance of the solution was then measured at a wavelength of 570 nm.

2.8. Statistical analysis

The statistical analysis was carried out using a one-way analysis of variance (ANOVA) with the aid of SPSS 20 software. A significance level of $p \leq 0.05$ was set to identify statistically significant differences. The mean ± standard deviation was utilized to present all quantitative data.

3. Results and discussion

This integration of NPs with cardiac patches holds promise to profoundly influence the material’s mechanical and adhesive properties, along with impacting tissue morphogenesis and guiding cell self-assembly in a three-dimensional setting [28–30]. Gold nanostructures have been identified as potential contenders in the field of biology, namely in areas such as tissue engineering and biosensing. This is due to their biocompatibility, inertness towards cells, and ability to exhibit localized surface plasmon resonance (LSPR) within the visible spectrum [31]. In the current project, we synthesized AuNPs via the green chemistry approach using oat extract as the reducing and capping agent. The synthesized AuNPs were characterized via standard and informative technique. Using the DLS technique we observed that the Oat-mediated AuNPs have a hydrodynamic size of 346 ± nm (Fig. 1A) and the zeta

measurement showed the average zeta potential of −29 mV (Fig. 1B). The observed zeta potential indicates that the Oat-mediated AuNPs have a suitable stability due to the high repulsive electrostatic interactions between NPs. It has been shown that suing green chemistry approach and natural substances, it is possible to synthesis AuNPs with different size. Mitra, M. et al. [32]. used terminalia arjuna to synthesis AuNPs and reported NPs with 20–40 nm in size. In another study, Mzwd, E. et al. used Gum Arabic and synthesized AuNPs with a size of 1.85 ± 0.99 nm [33].

The morphology of the Oat-mediated AuNPs was observed using TEM imaging (Fig. 2A) and SEM imaging (Fig. 2B). The results showed that the Oat-mediated AuNPs have a partially spherical morphology. Using the green chemistry approach, several studies have reported the synthesis of NPs with different morphologies. These possibilities are due to the fact that the synthesis of NPs involved various parameters, including the concentration of precursors, time of reaction, temperature of the reaction mixture, geometry of the reaction chamber, and the applied atmospheres. Ahmad, S. et al., reported Green synthesis of AuNPS with cubic geometry using *Delphinium Chitralense tuber* extracts [34].

The degree of crystallinity of the synthesized AuNPs was examined using XRD methodology, and the resulting XRD patterns are depicted in Fig. 3A. The gold nanocrystals demonstrated four discernible peaks at specific angles, namely 2θ = 38.1, 4.3, 64.5, and 77.7. Each of the four peaks observed in the data corresponds to the usual Bragg reflections of the (111), (200), (220), and (311) planes of a face-centered cubic (fcc) lattice [32,35,36]. The pronounced diffraction seen at the 38.1 peak indicates that the preferred growth orientation of zero valent gold was established along the (111) direction. The term "molecular-sized solids" pertains to the formation of solids at the molecular scale, characterized by a recurring three-dimensional arrangement of atoms or molecules, wherein each constituent portion is equidistant from one another. The presented XRD pattern exhibits characteristic features that are commonly observed in the XRD patterns of pristine gold nanocrystals. The observed results are in agreement with previous studies. Mitra et al. applied bark extract of Terminalia arjuna to synthesis green synthesis of AuNPs and observed that the AuNPs have a fcc structure [32]. In another study, Bumbudsanpharoke and Ko used unbleached kraft pulp to synthesis AuNPs. They reported that the AuNPs have fcc structure [36]. Ahmada et al. used crude basic alkaloidal portion of the tuber of *Delphinium chitralense* to synthesis green AuNPs. They showed that the AuNPs have a pure crystalline structure with intense peaks at 2θ = 38.5°, 44.8°, 66.5°, 78° and 82° which are related to the (111), (200), (220), (311) and (222) plane proving the fcc structure [34].

Using the UV–Vis spectroscopy (Fig. 3B), we evaluated the optical properties of the synthesized AuNPs. The results showed that the AuNPs exhibited a broad absorbance peak around at 544 nm. The observed peak can be related to the size dependent quantum mechanical phenomenon (SPR). Moreover, it reported that the location of SPR peak between wavelength of 500–600 nm confirmed the formation of AuNPs [32]. Mubeen et al. applied the green chemistry approach using *Citrullus colocynthis* (bitter apple) to synthesis AuNPs. They reported that the resulted AuNPs have the UV–Vis characteristic peak at the range of 531.5–541.5 nm [37].

The integration of gold nanostructures into macroporous scaffolds has the potential to augment the conductivity of the matrix and improve the transmission of electrical signals among heart cells. The utilization of the electrical characteristics of gold nanostructures played a significant role in enhancing the electrical communication between neighboring heart cells. The study involved the incorporation of gold nanowires into the pore walls of macroporous alginate scaffolds in order to enhance both the spatial and overall conductivity of the matrix. Upon culturing heart cells in the nanowired scaffolds, there was a noticeable enhancement in the expression of contractile and electrical coupling proteins. The utilization of nanowired matrices led to an enhancement in the transmission of electrical signals within the biomaterial, ultimately leading to the development of a cardiac patch that exhibits synchronous beating. Moreover, nanofibrous nanocomposite cardiac patch containing AuNPs can integrate the beneficial properties of nanofiborus patch with AuNPs. We incorporated the Oat-mediated AuNPs into PCL/Gel nanofibers and the SEM images (Fig. 4A and B) showed that the fabricated nanofibers were straight without any deformity and beads.

Various studies have integrated AuNPs with nanofibers for different applications. For nanosensor applications, Zhu et al. coated nanofibers with AuNPs [38]. They reported that the incorporation of AuNPs with nanofibers provided a sophisticated structure ideal for nanosensor applications. In another study, Huang et al. used polyvinylpyrrolidone/ethylcellulose to fabricate scaffolds by coaxial electrospinning and showed that the incorporation of AuNPs improved the scaffolds' porosity and mechanical properties [39].

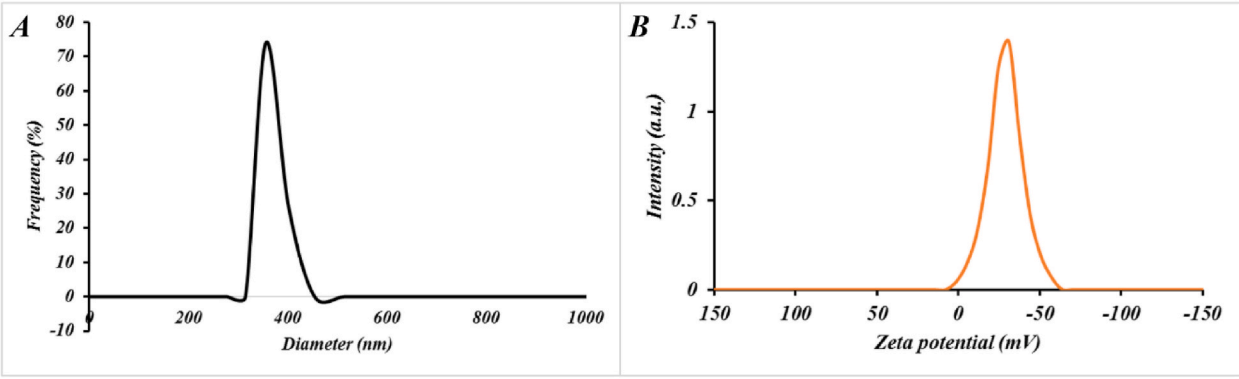

Fig. 1. (A) Hydrodynamic size distribution and (B) Zeta potential of the oat-mediated AuNPs. The oat-mediated AuNPs exhibit a hydrodynamic size measuring 346 ± nm. The zeta measurement revealed an average zeta potential of −29 mV.

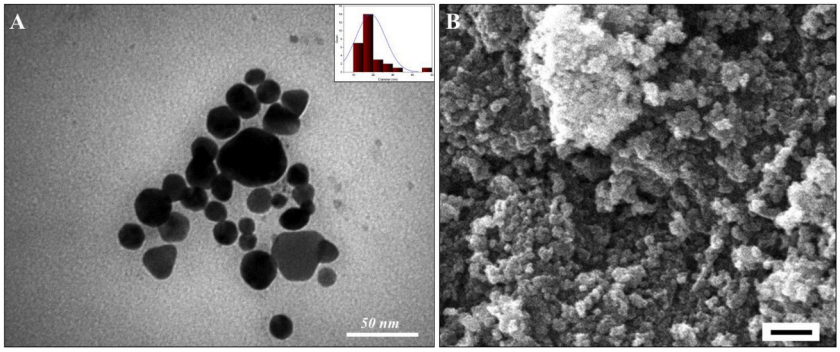

Fig. 2. The morphology of the oat-mediated AuNPs was examined using TEM (A) and SEM (B) imaging, which indicated a partially spherical shape for the particles.

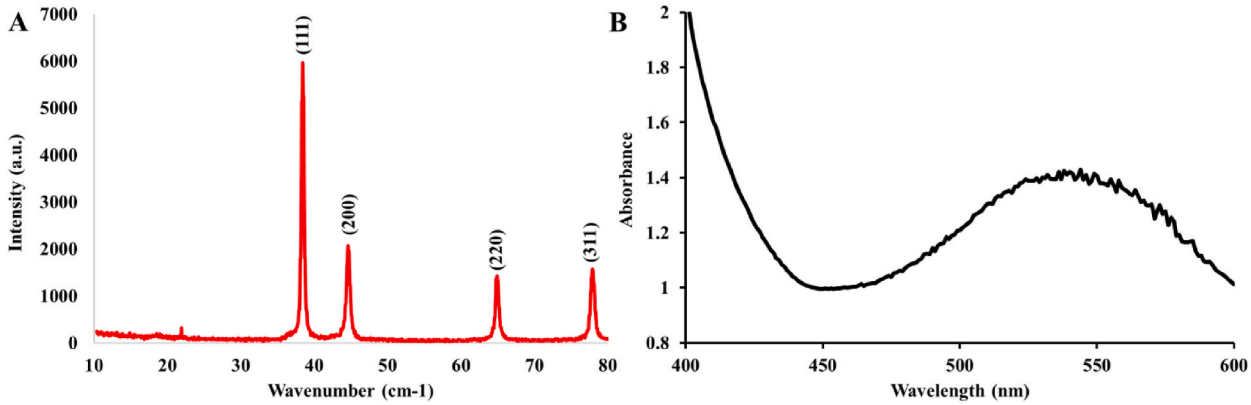

Fig. 3. (A)XRD pattern and (B) UV–Vis spectrum of the Oat-mediated AuNPs. The gold nanocrystals exhibited four distinct peaks at specific angles ($2\theta = 38.1$, 4.3, 64.5, and 77.7). Optical properties of the synthesized AuNPs were assessed using UV–Vis spectroscopy, revealing a broad absorbance peak around 544 nm. This observed peak can be attributed to the size-dependent quantum mechanical phenomenon (SPR).

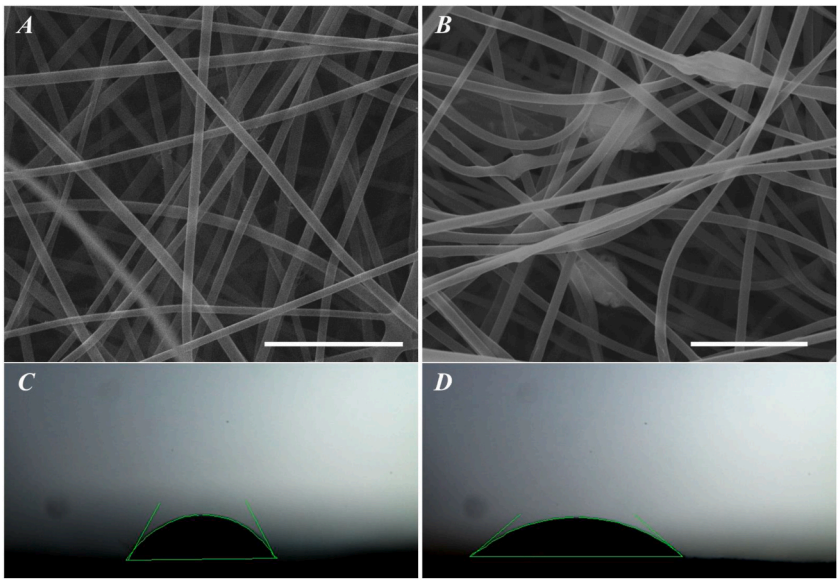

Fig. 4. Characteristics of the fabricated nanofibrous cardiac patches. (A) And (B) SEM images of PCL/Gel and PCL/Gel/AuNPs, respectively. (C) and (D) water contact angle images of PCL/Gel nanofibrous cardiac patch and PCL/Gel/AuNPs nanofibrous cardiac patch, respectively.

Table 1
Numerous research papers have combined AuNPs with nanofibers for diverse uses. Table 1 summarizes the qualities of certain environmentally friendly chemistry-produced AuNPs. These aspects cover the organic origin employed in nanoparticle synthesis, size, shape, surface charge, crystal structure, and the absorption peak of UV–Vis spectroscopy.

Studies	Bio-agent	Size (nm)	Morphology	Zeta potential (mV)	Crystalline structure	UV–Vis absorption peak (nm)
Our study	*Avena sativa* L. Extract	18.7 ± 7.4	Partially spherical	−29	Fcc structure	544
[32]	*Terminalia arjuna*	20–40	Spherical	NA	Fcc structure	524
[34]	*Delphinium chitralense*	100–300 nm	Cubic geometry	NA	Fcc structure	550–560
[37]	*Citrullus colocynthis*	7–33	Spherical	NA	Fcc structure	531.5–541.5
[40]	*Papaver somniferum*	77	Spherical	NA	NA	544
[33]	Gum Arabic	1.85 ± 0.99	Spherical	NA	NA	514–521
[41]	*Sarcophyton crassocaule*	5–50	Spherical	−22.129	NA	517
[42]	Tea leaf	31.16 ± 6.67	Nearly spherical and were with few triangular particles	−28.6	Metallic gold (JCPDS 00–001–1172)	571

NA: Not available.

Furthermore, they demonstrated that the fabricated scaffold exhibited excellent osteogenic bioactivity in vitro and *in vivo*. Table 1. Summarizes the characteristics of some green chemistry synthesized AuNPs.

Most frequently, low surface interactions with blood constituents are linked to hydrophilicity. On the other hand, it was discovered that when exposed to surface blood plasma, hydrophobic surfaces adsorb more proteins with a greater degree of protein conformational change [43]. Additionally, it can encourage cell adhesion and inflammatory responses. In turn, this may change the function and activity of the proteins. Protein expulsion from aqueous solution was described as protein adsorption to hydrophobic surfaces, which increases hydrogen bonding between water molecules. By doing so, less desirable interactions between water and proteins are sacrificed. WCA analysis can be used to evaluate the hydrophilicity of solid polymer film surfaces, which is predicted to increase upon biological surface oxidation. The results of WCA (Fig. 4C and D) showed that the integration of Oat-mediated AuNPs with PCL/Gel nanofibers reduced the WCA value from 61.8° (Fig. 4C) to 41° (Fig. 4D), indicating the improved hydrophilicity of nanofibers.

A substance is considered porous if it contains empty spaces, connections or passages between these empty spaces, and medium walls or supports that create a three-dimensional framework. Understanding the impact of a material's porosity on its performance requires considering its specific context. To support these environments and facilitate the removal of metabolic byproducts, the gaps in tissue-engineered scaffolds often enable cell movement, oxygen intake, and nutrient flow [44]. It is presumed that interstitial fluid is saturated in these voids. Drug transport promotes drug release by material breakdown or drug dispersion [45]. Porosity, pore size, and connectivity thus have a significant impact on the penetration qualities. Capillary action is a penetration mechanism that facilitates the entry of liquid into the pores. However, as the pore or throat size decreases, size limitations may hinder the penetration of certain materials like cells [45]. On the flip side, capillary action leads to increased fluid permeation over shorter distances when pores are smaller. Therefore, the properties of the target scaffolds and surface interactions play a significant role in how pore size affects liquid penetration. Porosity also affects the surface-area-to-volume ratio of the material, with increased porosity resulting in greater material surface area. Additionally, controlled porosity in large pores further decreases the material's surface area. The surface-area-to-volume ratio also needs to consider the size of the wall or strut. Materials with a high surface-to-volume ratio facilitate cell attachment and drug release. Moreover, the existence of pores implies the potential for inflammatory reactions, bacterial invasion, or platelet activation. For instance, the porosity of fabricated AuNPs-incorporated nanofibrous cardiac patches was measured to be in the range of 65–75 %, showcasing their porous nature (Fig. 5 A). Moreover, the incorporation of AuNPs has not significant effect on the porosity of the nanofibers. The swelling capacity of the fabricated patches was evaluated using the gravimetric method and the results are presented in Fig. 5B. The results showed that the nanofibers exhibited a time-dependent swelling and the highest swelling percentage was obtained at 36 h after incubation for both the patches. Moreover, the AuNPs-incorporated nanofibrous cardiac patch showed a higher swelling state than the pristine PCL/Gel nanofibers which can be due to the presence of AuNPs in the structure of nanofibers (Fig. 5 B).

Increasing evidence suggests that the primary cause of detrimental changes in the heart structure and the onset of long-term heart failure is hypoxia-induced oxidative stress resulting from an overabundance of reactive oxygen species (ROS). Therefore, essential treatments for repairing failing heart tissue and reviving cardiac function could involve reinstating oxygen supply and reducing oxidative stress. If this approach is ineffective, stimulating angiogenesis may help restore lost functionality [46–48]. In the etiology of heart damage following MI, ROS is a key player. Following MI, it has been noted that ROS significantly increases. When blood circulation is restored after an acute myocardial infarction, a condition known as ischemia reperfusion, oxidative stress also increases. The myocardium undergoes structural and functional alterations as a result of ROS modulating collagen production and fibroblast proliferation. Antioxidant-based therapeutic treatments have been proven to reduce heart remodeling and improve function [49]. As a result, reducing ROS may lessen harmful cardiac remodeling and improve heart function, improving the therapeutic result for the

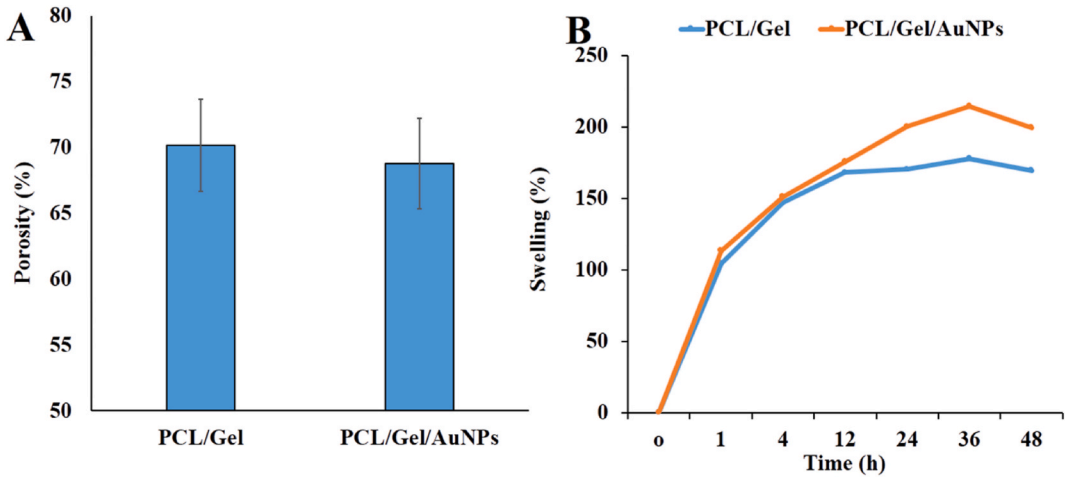

Fig. 5. (A) Porosity value of the fabricated nanofibrous cardiac patches and (B) Swelling state of the fabricated nanofibrous cardiac patches. The analysis of porosity in the developed AuNPs-infused nanofibrous cardiac patches revealed that these structures possess a porosity ranging from 65 to 75 %. Additionally, the AuNPs-infused nanofibrous cardiac patch exhibited greater swelling compared to the pristine PCL/Gel nanofibers, potentially attributable to the incorporation of AuNPs within the nanofiber structure.

treatment of MI. After a MI, one of the fundamental treatments involves reinstating oxygen supply to prevent tissue hypoxia, thus potentially averting cardiac cell death in the affected area. While certain clinical studies have reported no significant effects, others have indicated that exposing patients to 100 % oxygen can lessen the size of the infarct and enhance heart function. Similarly, research on oxygen-based therapies including direct injection of oxygen-supersaturated blood into the coronary artery and oxygen carrier infusions, in both preclinical and clinical settings, has demonstrated improved cardiac performance [50–53]. Accordingly, we applied the green chemistry synthesis approach to augment the antioxidant potential of AuNPs. The antioxidant potential of the Oat-mediated AuNPs was evaluated according the radical scavenging potential NPs against DPPH (Fig. 6 A), H_2O_2 (Fig. 6 B), and ONOO (Fig. 6C) free radicals. The results showed that the Oat-mediated AuNPs exhibited dose-dependent antioxidant properties. The observed radical scavenging against the tested oxidant can be due to the fact that during the synthesis of AuNPs via the green chemistry approach, the phytochemicals of *Avena sativa* L. act as the capping agent and elevated the radical scavenging potential of the NPs [54]. The antioxidant activity of the green synthesized AuNPs has been reported by other researchers. Shabestarian et al. used *sumac aqueous* extract to synthesis AuNPs and observed a dose-dependent radical scavenging activity against ABTS (2, 2′-azino-bis 3-ethylbenzthiazoline-6--sulfonic acid) and DPPH [55]. They proposed that the adsorption of the bio-compounds of the extract onto the surface of NPs is the main cause of the radical scavenging activities. Muthuvel et al. reported that Solanum nigrum leaf extract-mediated AuNPs exhibited a potent and dose-dependent DPPH radical and hydroxyl radical scavenging activities compared to the aqueous leaf extract of Solanum nigrum [56].

In the area of tissue engineering, the intentional and controlled release of pharmaceutical substances from a supportive structure can speed up local regeneration processes and alleviate concerns about potential negative effects of the pharmaceutical on the entire organism. For drugs to be effective, they must meet a specific minimum threshold. However, the limited duration of their presence in the body makes it difficult to administer a significant dosage at the specific site of injury over an extended period. This challenge arises

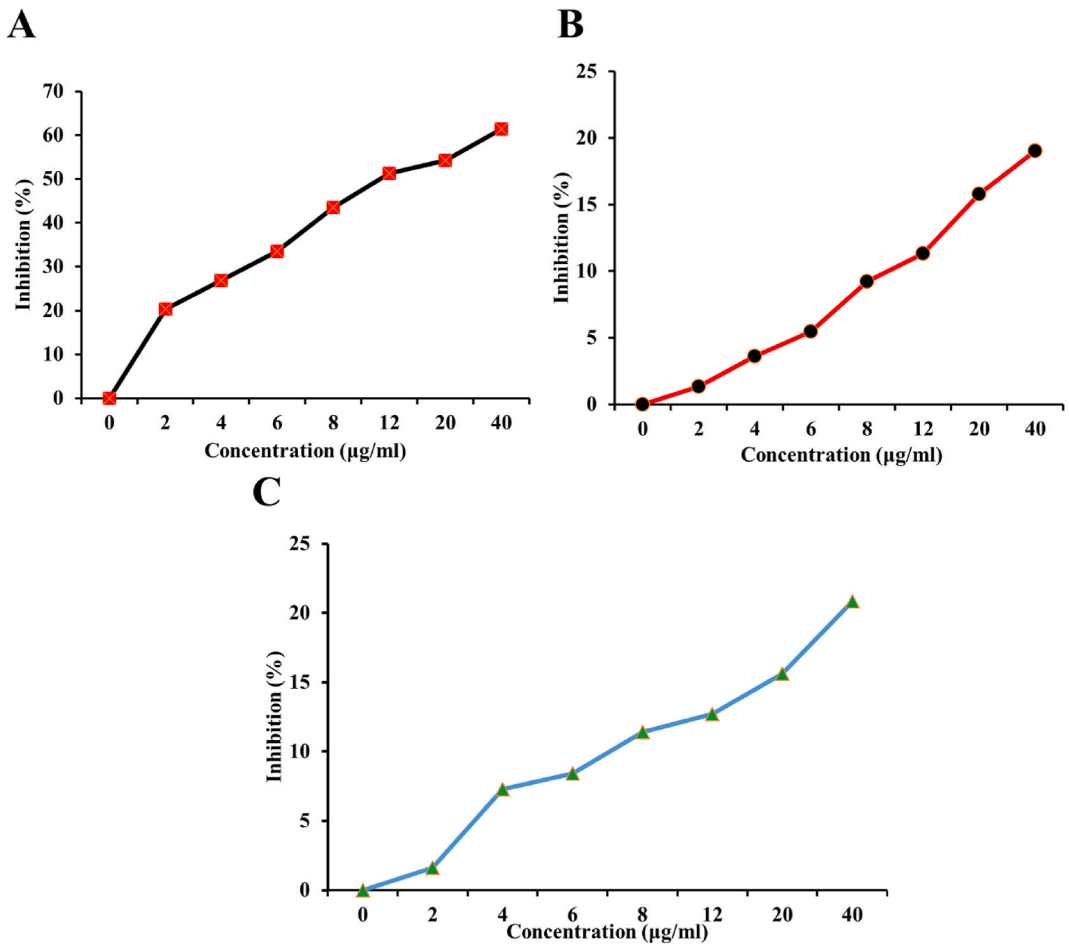

Fig. 6. Radical scavenging potential of the Oat-mediated AuNPs. (A) DPPH radical scavenging potential, (B) H_2O_2 radical scavenging potential, and (C) ONOO radical scavenging potential. The antioxidant properties of the Oat-mediated AuNPs depended on the dosage, as they exhibited dose-dependent behavior. The observed radical scavenging activity against the tested oxidant can be attributed to the phytochemicals of *Avena sativa* L. acting as a capping agent during the synthesis of AuNPs through the green chemistry approach, thereby boosting the radical scavenging potential of the nanoparticles.

from the potential adverse consequences of systemic drug delivery, which may result in excessive exposure of cells and tissues to the drug. The use of controlled drug release mechanisms within tissue engineering scaffolds facilitates the establishment of localized drug concentrations that are both therapeutically significant and sustained over prolonged durations. The field of controlled release encounters issues pertaining to the precise modulation of drug release, while simultaneously preserving the mechanical and structural integrity of the scaffold, and avoiding any detrimental effects or rapid depletion of the drug [57]. The results of release evaluation showed that the incorporated AuNPs released from the PCL/Gel nanofibrous cardiac patch (Fig. 7A). The drug release findings indicated rapid release within the first 10 h, facilitating enhanced and expedited drug bioavailability. Subsequently, the release becomes controlled, providing sustained release for up to 50 h following the initial rapid effect.

The effective use of blood-contacting biomaterials is constrained by hemocompatibility, which is a significant consideration. These materials come into direct contact with blood, a complex biological substance comprised of 55 % plasma, 44 % red blood cells, and 1 % white blood cells and platelets. Thus, it is essential to thoroughly assess potential adverse interactions between newly developed materials and blood to reduce the risk of triggering and harming blood components. The initial protein layer that attaches to the biomaterial's surface primarily triggers negative reactions, such as activating coagulation through the intrinsic pathway, stimulating inflammation by activating white blood cells, and promoting adhesion and activation of platelets (Liu et al., 2014). As a result, there might be a decrease in the number of blood cells, potentially leading to the formation of a blood clot. Thus, it is crucial that blood-contacting biomaterials used in practical applications do not elicit any adverse reactions with blood components, such as activation or destruction. Red blood cells, also known as erythrocytes, make up the majority of blood cells, typically ranging from 4 to 6 million cells per microliter. Their primary role is to transport oxygen (O_2) from the lungs to various tissues and cells while aiding in the movement of carbon dioxide (CO_2) from tissues back to the lungs. Erythrocytes, being the most rigid blood cells, are susceptible to rupture and hemolysis due to shear stress and changes in osmotic pressure. The hemocompatibility testing revealed that the manufactured cardiac patch resulted in less than 7 % hemolysis and is considered hemocompatible (Fig. 7B).

The term "biocompatibility" is frequently used to describe the appropriateness of a biomaterial or biomaterials used in a medical device to meet essential biological standards. Biocompatibility can be defined as the ability of a material to elicit an appropriate response from the host organism in a specific application. Assessing biocompatibility or safety involves determining an appropriate response from the host organism. We assessed the biocompatibility of the created nanofibrous cardiac patch through the MTT assay, and the findings are illustrated in Fig. 8. The results demonstrated that the use of Oat-mediated AuNPs did not produce significant toxicity and are considered to be biocompatible.

4. Conclusion

In conclusion, the field of cardiac tissue engineering has seen significant advancements through collaborative interdisciplinary efforts. The emphasis on mimicking the natural extracellular matrix in myocardium has led to the development and evaluation of various materials, with electrospun nanofibrous scaffolds emerging as a promising option. In this study we hypothesized that the combination of green/eco-friendly AuNPs with nanofibers may resulted in the fabrication of sophisticated cardiac patch. Accordingly, we used *Avena sativa* L. extract as the reducing and capping agent, during the synthesis of AuNPs. We observed that the results AuNPs exhibited outstanding and promising physical, chemical, and biological properties. Moreover, we integrated the synthesized AuNPs with nanofibers using the electrospinning technique and obtained a nanofibrous cardiac patch. Although we obtained promising results, the healing efficacy of the nanofibrous cardiac patch should be evaluated using proper animal model and molecular studies. Fog the future direction, it is possible to introduce the fabricated nanofibrous cardiac patch to the clinic and market after conducting proper animal models and passing the clinical trials.

Funding

Not applicable.

Informed consent

Not applicable.

Ethical approval

The conducted research is not related to either human or animal use.

Data availability

The datasets are available from the corresponding author on reasonable request.

CRediT authorship contribution statement

Xinfang Wei: Writing – original draft, Investigation, Formal analysis. **Xiaoshan Jiang:** Writing – review & editing, Methodology, Formal analysis. **Hongzan Li:** Writing – review & editing, Funding acquisition, Data curation, Conceptualization.

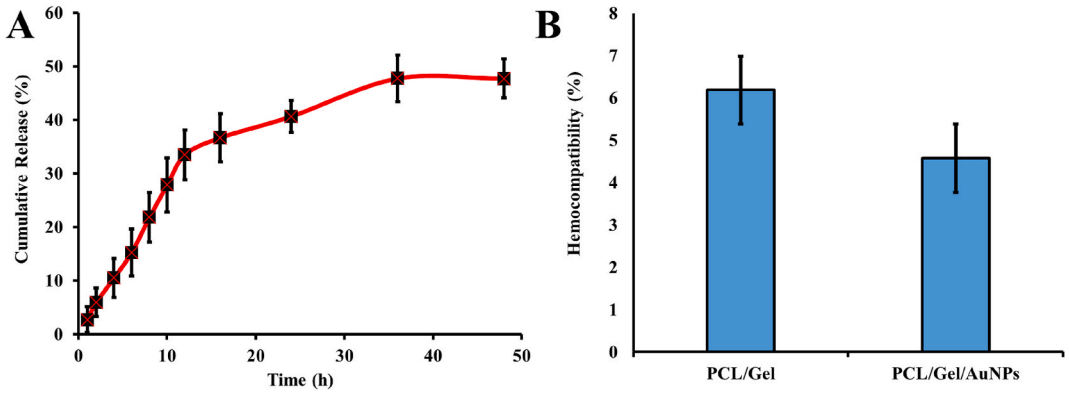

Fig. 7. (A) Cumulative release of the oat-mediated AuNPs from nanofibrous patch, the drug is quickly released within the initial 10 h, followed by a gradual and controlled release continuing for up to 50 h, and (B) Hemocompatibility of the cardiac patch, the hemocompatibility test results showed that the synthesized cardiac patch caused less than 7 % hemolysis and is considered hemocompatible.

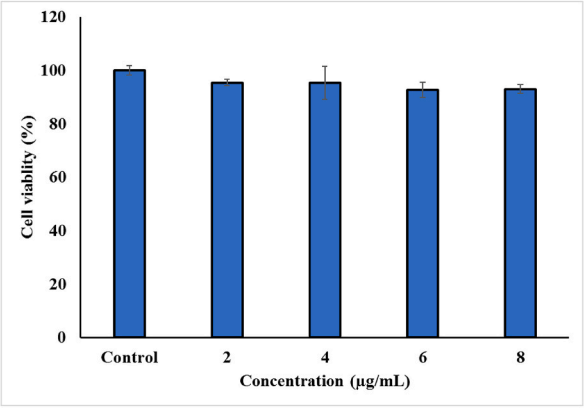

Fig. 8. The viability of the cells under incubation of the oat-mediated AuNPs. The findings indicated that the Oat-assisted AuNPs did not cause notable toxicity and are considered to be biocompatible.

Declaration of competing interest

The authors declare that they have no known competing financial interests or personal relationships that could have appeared to influence the work reported in this paper.

Acknowledgments

Not applicable.

References

[1] M. Lindstrom, et al., Global burden of cardiovascular diseases and risks collaboration, 1990-2021, J. Am. Coll. Cardiol. 80 (25) (2022) 2372–2425.
[2] D. Appiah, et al., Perceived neighborhood social cohesion and the 10-year risk of cardiovascular disease in low-and middle-income countries: the World Health Organization Study on Global Aging and Adult Health, Health Place 77 (2022) 102895.
[3] A.P. DeFilippis, et al., Atherothrombotic factors and atherosclerotic cardiovascular events: the multi-ethnic study of atherosclerosis, Eur. Heart J. 43 (10) (2022) 971–981.
[4] Q.M. Bui, et al., Psychosocial evaluation of candidates for heart transplant and ventricular assist devices: beyond the current consensus, Circulation: Heart Fail. 12 (7) (2019) e006058.
[5] N. Liu, et al., Advances in 3D bioprinting technology for cardiac tissue engineering and regeneration, Bioact. Mater. 6 (5) (2021) 1388–1401.
[6] G.I. Barbulescu, et al., Decellularized extracellular matrix scaffolds for cardiovascular tissue engineering: current techniques and challenges, Int. J. Mol. Sci. 23 (21) (2022) 13040.
[7] J.A. Roacho-Pérez, et al., Artificial scaffolds in cardiac tissue engineering, Life 12 (8) (2022) 1117.
[8] S. Mohammadi Nasr, et al., Biodegradable nanopolymers in cardiac tissue engineering: from concept towards nanomedicine, Int. J. Nanomed. (2020) 4205–4224.
[9] X. Chen, et al., Insight into heart-tailored architectures of hydrogel to restore cardiac functions after myocardial infarction, Mol. Pharm. 20 (1) (2022) 57–81.
[10] M.P. Prabhakaran, et al., Electrospun biocomposite nanofibrous patch for cardiac tissue engineering, Biomed. Mater. 6 (5) (2011) 055001.

[11] R. Ravichandran, et al., Elastomeric core/shell nanofibrous cardiac patch as a biomimetic support for infarcted porcine myocardium, Tissue Eng. 21 (7–8) (2015) 1288–1298.
[12] D. Kai, et al., Stem cell-loaded nanofibrous patch promotes the regeneration of infarcted myocardium with functional improvement in rat model, Acta Biomater. 10 (6) (2014) 2727–2738.
[13] A. Fakhrali, et al., Electro-conductive nanofibrous structure based on PGS/PCL coated with PPy by in situ chemical polymerization applicable as cardiac patch: fabrication and optimization, J. Appl. Polym. Sci. 139 (19) (2022) 52136.
[14] Y. He, et al., Mussel-inspired conductive nanofibrous membranes repair myocardial infarction by enhancing cardiac function and revascularization, Theranostics 8 (18) (2018) 5159.
[15] T. Gültan, M. Gümüşderelioğlu, Membrane supported poly (butylene adipate-co-terephthalate) nanofibrous matrices as cardiac patch: effect of basement membrane for the fiber deposition and cellular behavior, Colloids Surf. A Physicochem. Eng. Asp. 654 (2022) 129977.
[16] Z. Chang, et al., Preparation of gelatin/Ag NPs under ultrasound condition: a potent and green bio-nanocomposite for the treatment of pleomorphic hepatocellular carcinoma, morris hepatoma, and novikoff hepatoma, Arab. J. Chem. 15 (6) (2022) 103858.
[17] C.-W. Hsiao, et al., Electrical coupling of isolated cardiomyocyte clusters grown on aligned conductive nanofibrous meshes for their synchronized beating, Biomaterials 34 (4) (2013) 1063–1072.
[18] T. Dvir, et al., Nanowired three-dimensional cardiac patches, Nat. Nanotechnol. 6 (11) (2011) 720–725.
[19] A.E. Fazary, et al., Thermodynamic studies on metal ions–Ninhydrin–Glycine interactions in aqueous solutions, J. Chem. Therm. 118 (2018) 302–315.
[20] V.G. Kumar, et al., Facile green synthesis of gold nanoparticles using leaf extract of antidiabetic potent Cassia auriculata, Colloids Surf. B Biointerfaces 87 (1) (2011) 159–163.
[21] N. Li, et al., Synthesis of Au NPs/Quince nanoparticles mediated by Quince extract for the treatment of human cervical cancer: introducing a novel chemotherapeutic supplement, Materials Express 12 (12) (2022) 1465–1473.
[22] N. Amini, G. Amin, Z. Jafari Azar, Green synthesis of silver nanoparticles using *Avena sativa* L. extract, Nanomedicine Research Journal 2 (1) (2017) 57–63.
[23] V. Karthick, et al., Green synthesis of well dispersed nanoparticles using leaf extract of medicinally useful Adhatoda vasica nees, Micro Nanosyst. 4 (3) (2012) 192–198.
[24] N. Hamdan, et al., PCL/Gelatin/Graphene oxide electrospun nanofibers: effect of surface functionalization on in vitro and antibacterial response, Nanomaterials 13 (3) (2023) 488.
[25] M. Doostmohammadi, et al., Polycaprolactone/gelatin electrospun nanofibres containing biologically produced tellurium nanoparticles as a potential wound dressing scaffold: physicochemical, mechanical, and biological characterisation, IET Nanobiotechnol. 15 (3) (2021) 277–290.
[26] C. Ramamurthy, et al., The extra cellular synthesis of gold and silver nanoparticles and their free radical scavenging and antibacterial properties, Colloids Surf. B Biointerfaces 102 (2013) 808–815.
[27] S. Patil, P. Rajiv, R. Sivaraj, An investigation of antioxidant and cytotoxic properties of green synthesized silver nanoparticles, Indo American Journal of Pharmaceutical Sciences 2 (10) (2015) 1453–1459.
[28] M. Yadid, R. Feiner, T. Dvir, Gold nanoparticle-integrated scaffolds for tissue engineering and regenerative medicine, Nano Lett. 19 (4) (2019) 2198–2206.
[29] S. Vial, R.L. Reis, J.M. Oliveira, Recent advances using gold nanoparticles as a promising multimodal tool for tissue engineering and regenerative medicine, Curr. Opin. Solid State Mater. Sci. 21 (2) (2017) 92–112.
[30] M. Borzenkov, et al., Gold nanoparticles for tissue engineering, Environmental Nanotechnology 1 (2018) 343–390.
[31] H. Hassan, et al., Gold nanomaterials–The golden approach from synthesis to applications, Mater. Sci. Energy Technol. 5 (2022) 375–390.
[32] M. Mitra, et al., Protective Role of Green Synthesized Gold Nanoparticles Using Terminalia Arjuna against Acetaminophen Induced Hematological Alterations in Male Wistar Rats, 2019.
[33] E. Mzwd, et al., Green synthesis of gold nanoparticles in Gum Arabic using pulsed laser ablation for CT imaging, Sci. Rep. 12 (1) (2022) 10549.
[34] S. Ahmad, et al., Green synthesis of gold nanaoparticles using Delphinium Chitralense tuber extracts, their characterization and enzyme inhibitory potential, Braz. J. Biol. 82 (2022) e257622.
[35] S. Krishnamurthy, et al., Yucca-derived synthesis of gold nanomaterial and their catalytic potential, Nanoscale Res. Lett. 9 (2014) 1–9.
[36] N. Bumbudsanpharoke, S. Ko, In-situ green synthesis of gold nanoparticles using unbleached kraft pulp, Bioresources 10 (4) (2015) 6428–6441.
[37] B. Mubeen, et al., Phytochemicals mediated synthesis of AuNPs from citrullus colocynthis and their characterization, Molecules 27 (4) (2022) 1300.
[38] H. Zhu, J.-F.o. Masson, C.G. Bazuin, Templating gold nanoparticles on nanofibers coated with a block copolymer brush for nanosensor applications, ACS Appl. Nano Mater. 3 (1) (2019) 516–529.
[39] C. Huang, et al., Gold nanoparticles-loaded polyvinylpyrrolidone/ethylcellulose coaxial electrospun nanofibers with enhanced osteogenic capability for bone tissue regeneration, Mater. Des. 212 (2021) 110240.
[40] M. Wali, et al., Green synthesis of gold nanoparticles and their characterizations using plant extract of Papaver somniferum, Nano Sci. Nano Technol. 11 (2017) 118.
[41] S. Rokkarukala, et al., One-pot green synthesis of gold nanoparticles using Sarcophyton crassocaule, a marine soft coral: assessing biological potentialities of antibacterial, antioxidant, anti-diabetic and catalytic degradation of toxic organic pollutants, Heliyon 9 (3) (2023) e14668.
[42] S. Patra, A.K. Golder, R.V. Uppaluri, Monodispersed AuNPs synthesized in a bio-based route for ultra selective colorimetric determination of Ni (II) ions, Chemical Physics Impact 7 (2023) 100388.
[43] X. Chen, J. Chen, N. Huang, The structure, formation, and effect of plasma protein layer on the blood contact materials: a review, Biosurface and Biotribology 8 (1) (2022) 1–14.
[44] N. Annabi, et al., Controlling the porosity and microarchitecture of hydrogels for tissue engineering, Tissue Eng., Part B 16 (4) (2010) 371–383.
[45] J. Braunecker, et al., The effects of molecular weight and porosity on the degradation and drug release from polyglycolide, Int. J. Pharm. 282 (1–2) (2004) 19–34.
[46] J. Ding, et al., A reactive oxygen species scavenging and O2 generating injectable hydrogel for myocardial infarction treatment in vivo, Small 16 (48) (2020) 2005038.
[47] A. Nabeebaccus, M. Zhang, A.M. Shah, NADPH oxidases and cardiac remodelling, Heart Fail. Rev. 16 (2011) 5–12.
[48] T.-H. Cheng, et al., Involvement of reactive oxygen species in angiotensin II-induced endothelin-1 gene expression in rat cardiac fibroblasts, J. Am. Coll. Cardiol. 42 (10) (2003) 1845–1854.
[49] X. Wang, et al., Ag nanoparticles immobilized on guanidine modified-KIT-5 mesoporous nanostructure: evaluation of its catalytic activity for synthesis of propargylamines and investigation of its antioxidant and anti-lung cancer effects, Arab. J. Chem. 15 (2) (2022) 103548.
[50] K. Sugamura, J.F. Keaney Jr., Reactive oxygen species in cardiovascular disease, Free Radic. Biol. Med. 51 (5) (2011) 978–992.
[51] F.J. Pashkow, D.G. Watumull, C.L. Campbell, Astaxanthin: a novel potential treatment for oxidative stress and inflammation in cardiovascular disease, Am. J. Cardiol. 101 (10) (2008) S58–S68.
[52] E.G. Rosenbaugh, et al., Antioxidant-based therapies for angiotensin II-associated cardiovascular diseases, Am. J. Physiol. Regul. Integr. Comp. Physiol. 304 (11) (2013) R917–R928.
[53] J.G. Farías, et al., Antioxidant therapeutic strategies for cardiovascular conditions associated with oxidative stress, Nutrients 9 (9) (2017) 966.
[54] A. Vinodhini, et al., Cardioprotective potential of biobased gold nanoparticles, Colloids Surf. B Biointerfaces 117 (2014) 480–486.
[55] H. Shabestarian, et al., Green synthesis of gold nanoparticles using sumac aqueous extract and their antioxidant activity, Mater. Res. 20 (1) (2016) 264–270.
[56] A. Muthuvel, et al., Biosynthesis of gold nanoparticles using Solanum nigrum leaf extract and screening their free radical scavenging and antibacterial properties, Biomedicine & Preventive Nutrition 4 (2) (2014) 325–332.
[57] J. Hu, P.X. Ma, Nano-fibrous tissue engineering scaffolds capable of growth factor delivery, Pharmaceut. Res. 28 (2011) 1273–1281.